Edelweiss Applied Science and Technology
ISSN: 2576-8484
Vol. 9, No. 5, 2700-2716
2025
Publisher: Learning Gate
DOI: 10.55214/25768484.v9i5.7585

Stackable pallet-shaped triboelectric nanogenerator for water wave energy harvesting

Tong Jun Yang[1], Lim Way Soong[2*], Yeo Boon Chin[3], Calven Chin[4], Liew Kia Wai[5], Pee Pocherd[6], Nophadon Wiwatcharagoses[7]
[1,2,3,4,5,6]Faculty of Engineering and Technology, Multimedia University, Jalan Ayer Keroh Lama,75450 Melaka. Malaysia; wslim@mmu.edu.my (L.W.S.).
[7]Department of Electrical and Computer Engineering, King Mongkut University of Technology North Bangkok, Thailand.

Abstract: Water wave energy is a vast and underutilized renewable resource. It has the potential to power distributed devices in marine environments. Triboelectric nanogenerators (TENGs) have emerged as a reliable technology for harvesting low-frequency and irregular mechanical energy from natural sources like ocean waves. Herein, a stackable pallet-shaped triboelectric nanogenerator (SP-TENG) is proposed for water wave energy harvesting. The SP-TENG is based on a stackable pallet-inspired structure, offering a modular and scalable platform for converting low-frequency motion into usable electrical energy. By utilizing the solid-solid freestanding triboelectric layer mode, the SP-TENG is able to generate electricity through periodic contact and separation between triboelectric materials. In this paper, two different types of SP-TENGs are designed and tested, each using different triboelectric material configurations in the sliding components. Polytetrafluoroethylene (PTFE) and aluminum were chosen for their strong triboelectric polarity difference, which enables efficient charge generation. One prototype uses solid PTFE plates, while the other uses aluminum-coated sliding components. The main goal is to compare their performance in energy generation under simulated wave conditions. All experiments were conducted using manual sliding motion at approximately 1 Hz to mimic low-frequency wave excitation. The maximum voltage achieved by the best-performing SP-TENG is 4 V. An SP-TENG is able to power 93 LEDs as well as other small electronic devices. Therefore, the SP-TENG is proven to be an effective solution for harvesting water wave energy and powering various marine applications in the future.

Keywords: *Multi-layered structure, Pallet shape, Performance optimization, Triboelectric nanogenerator, Water wave energy harvesting.*

1. Introduction

As the world confronts many environmental challenges including energy shortage and environmental pollution, renewable energy has been proposed as a worldwide crucial solution to reduce the dependence on non-renewable energy. For example, the consumption and overexploitation of fossil fuels has increased in these few years and as a result of excessive combustion of fossil fuels, greenhouse gas emissions have increased drastically. Therefore, to address the depletion of fossil fuels and resolve environmental problem, human discovered various sustainable energy solutions to fulfil the increasing demand for power. Among the energy sources, ocean also known as a blue energy source which occupies 71% of the surface area of Earth. It can harvest wave energy, tidal energy and etc which considered as potential competitor in clean energy development and present abundant renewable energy source [1].

Traditionally, wave energy is harvested from electromagnetic induction generator (EMG). However, EMG faces several challenges such as high production cost, prone to corrosion, and low efficiency in power conversion especially in ocean waves where usually at a low frequency [2-4]. In

History: Received: 17 March 2025; Revised: 30 April 2025; Accepted: 6 May 2025; Published: 27 May 2025
* Correspondence: wslim@mmu.edu.my

2012, one of the emerging technologies of renewable energy to replace EMG as new ocean wave energy which is the Triboelectric Nanogenerator (TENG). Unlike EMG, TENGs utilize the triboelectric effect where the process in which certain materials become electrically charged after contacting with another material. When it is applied to harvest ocean wave energy, this fundamental mechanism offers TENGs to harvest power from mechanical energy generated by waves and transferring it into electricity through controlled friction as well as separation of materials [5, 6]. As compared to EMG, TENGs able to generate higher performance and efficiency of power and also drive a wide range of application. For example, TENGs can harness energy through different types of mechanical movements including vibrations [7], wind power [8] human motions [9] and water waves [10]. Also, TENGs able to power small electronic devices, sensors, and even contribute to larger energy systems.

There are five types of existing working interface of TENGs such as liquid-gas [11], solid-solid [12] liquid-liquid [13] solid-liquid [14] and solid-gas [15]. To harvest wave energy, two common ways are solid-solid interface and liquid-solid interface. In 2019, Wang et al. discovered the movement of electrons is an essential role for surface charge generation in solid-solid contacting mode [16]. When interatomic distances are reduced below the bonding length, allowing electron cloud overlap under mechanical stress. This process is named as Wang transition where this overlap lowers down the potential barrier and facilitates electron transition. The solid-solid contact mode represents one of the most efficient configurations in TENG operation. By repetitive contact and remove of two dissimilar materials, this mechanism produces alternating voltage that induces electrons movement within electrodes and then generates electrical power. On the other hand, solid-liquid contacting TENGs are isolated through the contact with water. However, in solid-liquid TENG, the triboelectric material is prone to damage and corrosion especially when in contact with water or submerged in it [17]. Therefore, researchers tend to concentrate on solid-solid contact mode in terms of choice of materials, surface properties, structural designs and applications.

The working mode of solid-solid contacting TENGs consists of four different types. The fundamental operation method including vertical contact-separation [18, 19] lateral sliding [20, 21] single-electrode [22, 23], and freestanding triboelectric-layer [24, 25]. Among these four working modes, this paper focuses on the freestanding triboelectric-layer mode where it involves a free moving triboelectric layer together with two electrodes without any direct electrical interconnection among each other. This mode can work in either sliding or contact separation configurations. This triboelectric layer moves between the two electrode and further inducing charge transfer due to the varying electrostatic field. Therefore, an electricity is generated in the circuit. This innovative mode is widely used in various fields, especially for energy harvesting from irregular mechanical motions. For example, freestanding TENGs are often applied in open environments like ocean buoys and wind-based systems, where they offer better adaptability to unpredictable and low-frequency movements, making them well-suited for marine energy harvesting.

Recently, several studies have focused on wave energy harvesting using TENGs, especially in exploring multi-layered structural designs and the selection of suitable triboelectric materials to enhance output performance. Wang, et al. [26] presented sandwich-like TENG (S-TENG) and integrated into a buoy system with the capability in harvesting wave energy [26]. The mechanism of S-TENG utilizes free rolling PTFE balls between acrylic plates and produced scalable output by stacking up to 70 layers. Under various wave conditions, S-TENG has resulted excellent adaptability and real-world application potential. Wang et al. developed a stackable TENG using rolling PTFE balls in multi-channel layers to harvest wave energy [27]. It offers modularity and improved directional adaptability but structural complexity at larger scales may be needed to improve. Zhang, et al. [28] designed a multi-tunnel triboelectric nanogenerator (MT-TENG) to harvest wave energy from marine floating bodies Zhang, et al. [28]. MT-TENG consisted novel structure with multiple semi-cylindrical tunnels that guide PTFE balls to move efficiently between copper electrodes. The energy harvesting performance is improved as compared to flat-type designs and demonstrating practical applications for powering LEDs on life buoys. Duan, et al. [29] proposed a scalable rolling-structured triboelectric

Edelweiss Applied Science and Technology
ISSN: 2576-8484
Vol. 9, No. 5: 2700-2716, 2025
DOI: 10.55214/25768484.v9i5.7585

nanogenerator (SR-TENG) for harvesting ocean energy [29]. To improve ocean energy harvesting, SR-TENG is optimized in the aspects of external shape and internal pellet filling to achieve enhanced power density.

Inspired by these previous studies, a stackable pallet-shaped triboelectric nanogenerator (SP-TENG) is proposed for water wave energy harvesting. Every layer of the SP-TENG is fabricated by 3D printer machine. On top of each layer, it is coated with aluminum electrode and three polytetrafluoroethylene (PTFE) plate on it. A SP-TENG consist of 11 stacks and they are parallel connected layers. Owing to their stackable feature, the output performance is increased. In this study, two prototypes of the triboelectric nanogenerator are built using different triboelectric material combinations. The goal is to test and compare their performance in generating electricity from wave motion. Various measurements such as voltage and capacitors charging rate are recorded and analyzed. All experimental results are based on a controlled manual-sliding motion at approximately 1 Hz to simulate wave excitation. Based on the results, the prototype with the best performance will be selected for further discussion and improvement. This comparison helps to better understand effect of material choices on energy harvesting efficiency and guides the future development of more effective TENG designs.

2. Experimental Setup

2.1. Hardware Structure

To study the performance of different triboelectric materials for wave energy harvesting, two types of sliding plate-based TENGs were developed. The first design is named SP-TENG-A, while the second configuration is referred to as SP-TENG-B for comparison purposes. Both prototypes consisted of 11 layers, and each layer was fabricated using additive manufacturing with polylactic acid (PLA) as the structural material. The first layer of the structure functions as a cover to enclose the internal components. In this study, aluminum and PTFE were selected as the triboelectric material pair where aluminum being naturally positive and PTFE being strongly negative in the triboelectric series [30]. This difference in electron affinity allows them to become oppositely charged during contact, making them suitable for efficient charge generation. Inside the devices, sliding plates move back and forth, creating repeated contact and separation between two triboelectric materials. As a result, electrical energy is generated. This multi-layered sliding mechanism was designed to enhance energy output under low-frequency wave motion. Figure 1 shows the outer structure of SP-TENG.

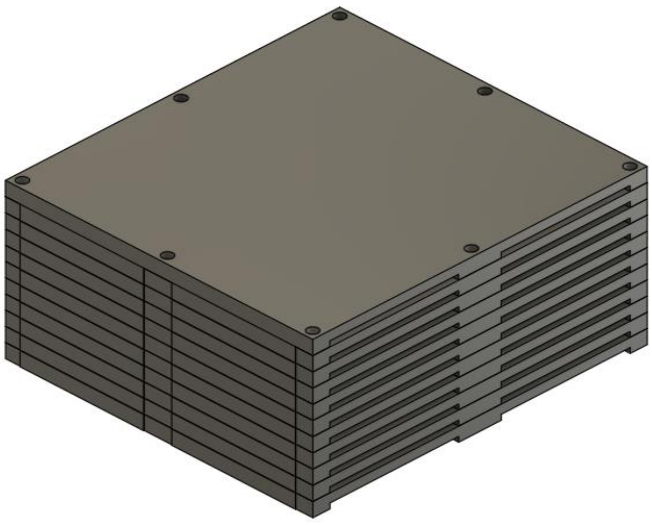

Figure 1.
Outer structure of SP-TENG.

Edelweiss Applied Science and Technology
ISSN: 2576-8484
Vol. 9, No. 5: 2700-2716, 2025
DOI: 10.55214/25768484.v9i5.7585

The SP-TENG-A composed of 11 layers of rectangular pieces. Each layer is designed with dimensions of 11.75 cm in length and 10.8 cm in width. The thickness of the plate is 5.5 mm. It features six uniformly distributed circular holes, located at each corner and at the centre of both longer sides. These holes are designed to accommodate M3 screws. For fastening, six stainless steel M3 hexagon socket cap screws, each with a length of 7 cm, are used to securely attach the layers together. This configuration supports precise alignment and stable stacking in a multi-layer triboelectric nanogenerator structure. Every layer of SP-TENG consists of aluminum tapes serving as fixed electrodes, with an additional layer of PTFE tape coated on top as the triboelectric material. This configuration enhances surface charge generation during sliding contact and separation. Inside SP-TENG, a total of 30 sliding plates were fabricated using PLA through 3D printing. Each plate measures 4.7 cm × 3.35 cm with a thickness of 0.3 cm. The bottom surface of each sliding plate is coated with aluminum tape, which functions as the moving electrode in the triboelectric system. Figure 2 shows the internal structure of SP-TENG-A.

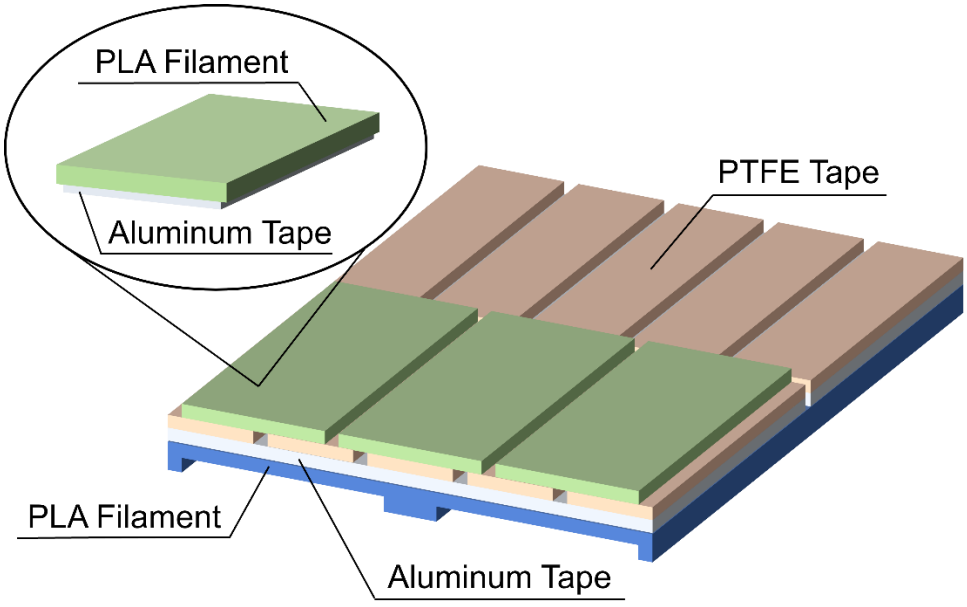

Figure 2.
Internal structure of SP-TENG-A.

Another similar structure of the SP-TENG was fabricated with a different material configuration. The fixed electrodes of SP-TENG-B remain stationary and are made from aluminum tape, which is applied to the top surface of each layer, but without any PTFE tape coating. In this version, the sliding plates are replaced with solid PTFE plates, serving as the moving triboelectric layer. The dimensions of the sliding plates remain the same as those used in the SP-TENG-A design. Figure 3 shows the internal structure of SP-TENG-B. In short, SP-TENG-A uses PLA sliding plates coated with aluminum and PTFE tapes, while SP-TENG-B replaces the sliding plates with solid PTFE plates and omits the PTFE layer on the fixed aluminum electrodes.

Edelweiss Applied Science and Technology
ISSN: 2576-8484
Vol. 9, No. 5: 2700-2716, 2025
DOI: 10.55214/25768484.v9i5.7585

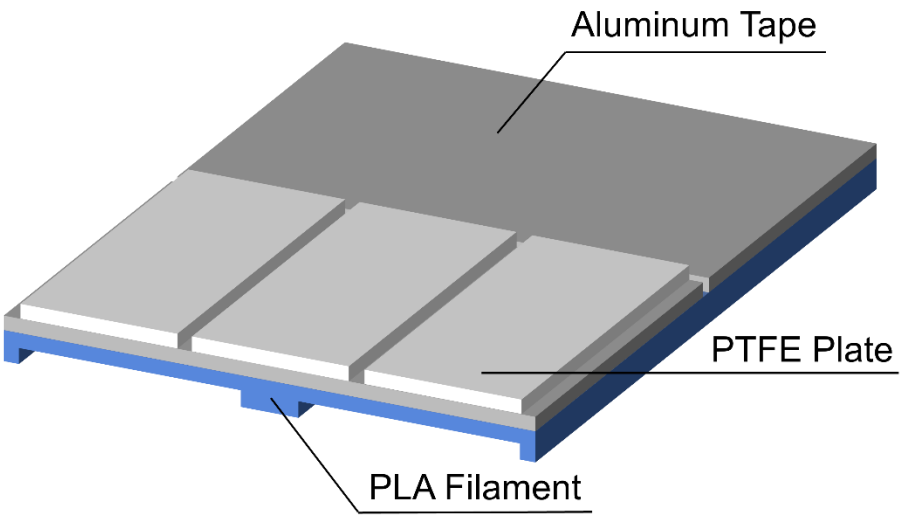

Figure 3.
Internal structure of SP-TENG-B.

2.2. Working Principle

The working principle of SP-TENG-A is shown in Figure 4. This device operates in freestanding triboelectric-layer mode, where the top aluminum-coated sliding plates act as moving electrodes, while the PTFE and bottom aluminum layers remain stationary. The complete operating cycle of TENG can be explained in four stages. In phase (i), when the aluminum-coated sliding plates are aligned with the PTFE layers, natural triboelectric contact causes electrons to transfer from aluminum to PTFE. As a result, the PTFE surface becomes negatively charged, and the aluminum becomes positively charged. This creates an electrostatic field. The opposite fixed aluminum electrodes beneath the PTFE then become induced with negative charges due to the influence of the positive charges in the moving aluminum-coated sliding plates. In phase (ii), as the aluminum-coated sliding plates move toward the right, the overlap between PTFE and aluminum changes. This imbalance causes a potential difference between the two fixed electrodes. Electrons flow from one electrode to the other through the external resistor (R), producing a current (I) in the circuit. In phase (iii), when the aluminum-coated sliding plates slides all the way to the right, it is now fully in contact with the PTFE layer on the right side electrodes. Now, the right fixed electrode becomes positively induced, while the left fixed electrode becomes negatively induced. At this point, the charge separation is at its maximum. In phase (iv), as the aluminum-coated sliding plates slides back to the left, the PTFE-aluminum contact and separation again shift. The direction of the potential difference reverses, and the electrons flow back through the resistor in the opposite direction. This creates an alternating current (AC) output. By manually sliding the plates, which resembles wave excitation, the overall process continues with each back-and-forth motion. Power is generated due to the natural triboelectric difference between aluminum and PTFE.

Edelweiss Applied Science and Technology
ISSN: 2576-8484
Vol. 9, No. 5: 2700-2716, 2025
DOI: 10.55214/25768484.v9i5.7585

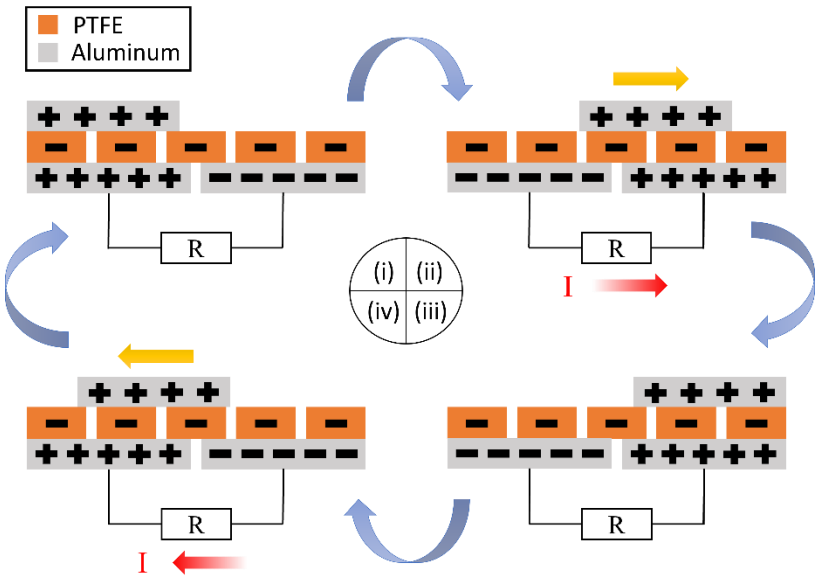

Figure 4.
Working principle of SP-TENG-A.

The working principle of SP-TENG-A is shown in Figure 5. The SP-TENG-B works in freestanding triboelectric-layer mode as well. It consists two aluminum layers as electrodes but PTFE plates are used for moving triboelectric layer. The complete operating cycle of TENG can be elaborated in four stages. In phase (i), the PTFE plate is fully aligned with the left aluminum electrode. Due to natural triboelectric contact, the negative charges on the PTFE plates attract positive charges to accumulate on the left electrode beneath them. Meanwhile, the opposite right electrode holds an equal-amount of negative charges. The system is in an electrostatically balanced state, and no current flows yet. In phase (ii), as the PTFE plate slides to the right, the overlap with the left electrode decreases, while the right electrode starts to become covered. This shift breaks the electrostatic balance and creates a potential difference between the two aluminum electrodes. Electrons flow from the right electrode to the left through the external resistor (R), generating a current (I) in the circuit. In phase (iii), when the PTFE fully overlaps with the right aluminum electrode, charge separation reaches its maximum, but the charge distribution becomes opposite to the initial state. The positive charge on the right electrode is strongest, and the left electrode becomes relatively negative due to electrostatic induction. The system again becomes momentarily balanced, and current flow stops. In phase (iv), as the PTFE slides back toward the left, the overlapping area shifts again, reversing the electrostatic potential difference. This causes electrons to flow back in the opposite direction through the resistor, generating a reverse current. This completes a full cycle of alternating current (AC) generation. The design utilizes the strong electron affinity of PTFE and the positive nature of aluminum to maximize charge generation and efficient energy harvesting.

Edelweiss Applied Science and Technology
ISSN: 2576-8484
Vol. 9, No. 5: 2700-2716, 2025
DOI: 10.55214/25768484.v9i5.7585

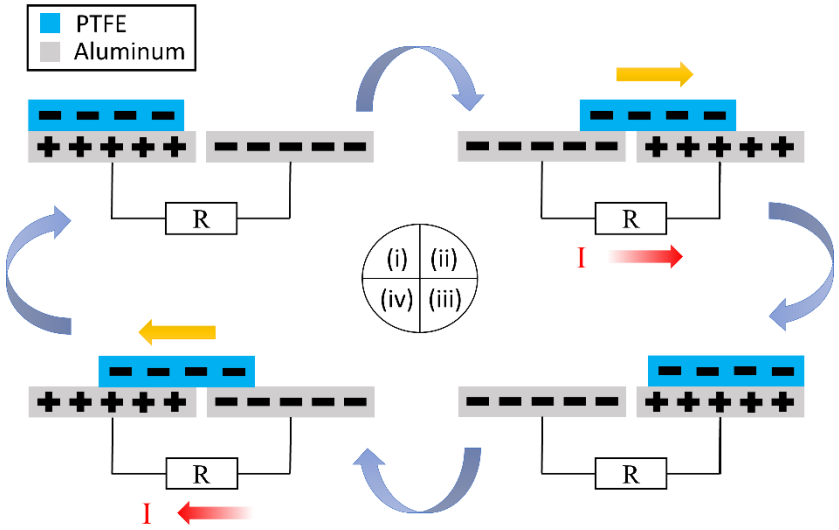

Figure 5.
Working principle of SP-TENG-B.

2.3. Circuit Design

SP-TENG generates an alternating current (AC) output through sliding motion. Figure 6 shows the circuit diagram of the SP-TENG. It is connected to a full-wave bridge rectifier (D1–D4), which converts the AC output from the TENG into DC. Four 1N4007 diodes are used in the rectifier circuit to ensure efficient rectification and reverse voltage protection.

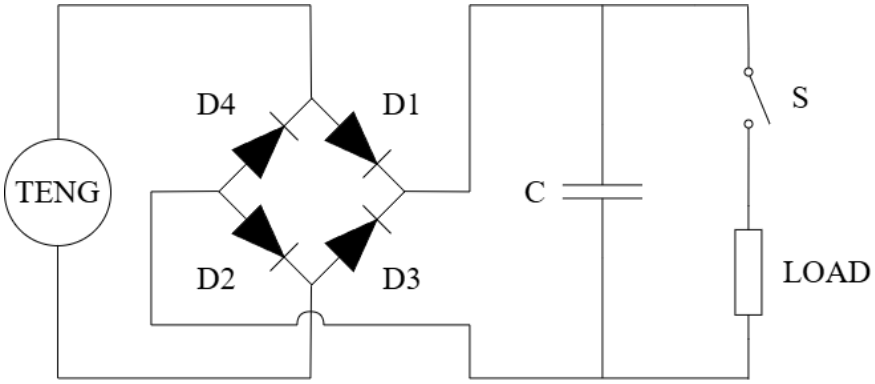

Figure 6.
Circuit diagram of the SP-TENG structure with the load or capacitor.

The rectified current charges a capacitor (C) to serve as energy storage. A switch (S) controls the discharge of this stored energy to an external load. When S1 is closed, the capacitor releases the energy to power the load. This setup enables efficient energy harvesting and management from the sliding motion of the SP-TENG.

3. Result and Discussion

The electrical output performance of the SP-TENG was analyzed by measuring the open-circuit voltage (VOC) in both AC and DC forms, and evaluating the capacitor charging time. All these parameters were measured by simulated wave motion through manual sliding movement at 1 Hz of frequency. The SP-TENG was consistently tested at a tilt angle of 50° to simulate inclined wave

Edelweiss Applied Science and Technology
ISSN: 2576-8484
Vol. 9, No. 5: 2700-2716, 2025
DOI: 10.55214/25768484.v9i5.7585

motion. These analyses help to determine the energy conversion efficiency and storage capability of the SP-TENG system. As shown in Figure 7, SP-TENG-A achieved an average positive peak voltage of +3.02 V and negative peak voltage of -3.08 V under 1 Hz frequency. It demonstrated a nearly symmetrical charge separation during triboelectrification. The minimal deviation between positive and negative peaks is ±0.06 V. However, the voltage waveform shows clear distortion, indicating instability in the output signal.

The DC voltage of SP-TENG-A is illustrated in Figure 8. SP-TENG-A is connected to a full-bridge rectifier to rectify the AC signal generated during periodic contact-separation cycles of the triboelectric materials. It is observed that a stable DC output with an average positive peak of 3.72 V is produced. The near-constant voltage level over the 10-second timeframe indicates minimal ripple and efficient charge retention. This is due to the ability of rectifier to mitigate AC fluctuations while preserving energy.

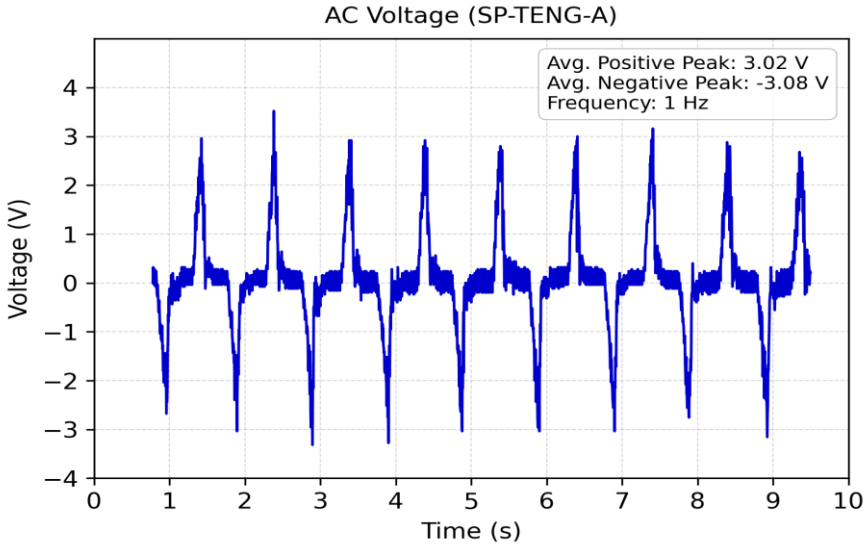

Figure 7.
AC Voltage of SP-TENG-A.

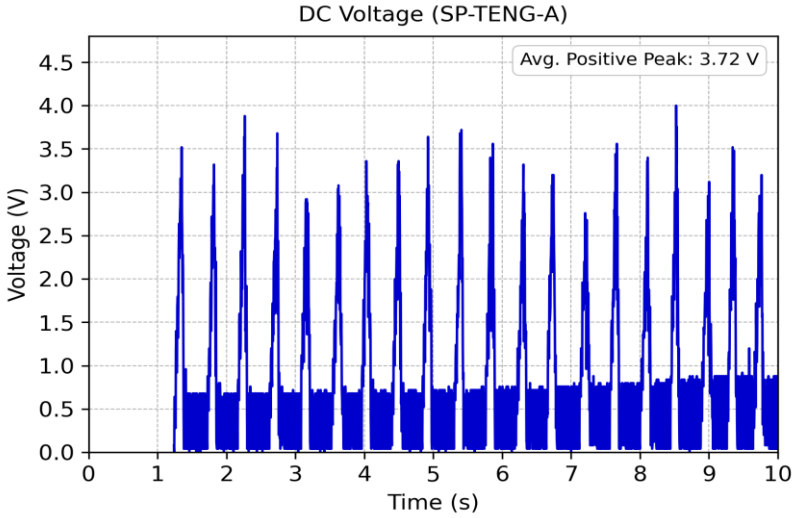

Figure 8.
DC Voltage of SP-TENG-A.

Edelweiss Applied Science and Technology
ISSN: 2576-8484
Vol. 9, No. 5: 2700-2716, 2025
DOI: 10.55214/25768484.v9i5.7585

The AC open-circuit voltage (VOC) of SP-TENG-B is presented in Figure 9. SP-TENG-B produced an average positive peak voltage of +3.14 V and negative peak voltage of -3.13 V under 1 Hz frequency. As compared to SP-TENG-A, it achieved completely symmetrical charge separation during triboelectrification. The deviation between positive and negative peaks is smaller than SP-TENG-B which resulted ±0.01 V. This underscores reliability and efficient charge transfer dynamics of SP-TENG-B. From the regular pattern of the voltage oscillations, the voltage distortion of SP-TENG-B is lesser than SP-TENG-A. Therefore, SP-TENG-B has an efficient energy conversion with minimal distortion as compared to SP-TENG-A.

Figure 10 shows the DC voltage of SP-TENG-B. It produced a stable DC output with an average positive peak of 3.84 V. The produced DC voltage is slightly higher than SP-TENG-A. From the voltage waveform, it is observed that SP-TENG-B has a smaller ripple than SP-TENG-A. This may be caused by SP-TENG-B creates a better charge density and dielectric performance as compared to SP-TENG-A. As a result, the magnitude of generated charges during triboelectrification will be increased. This provides a stronger baseline signal for rectification, reducing the relative impact of residual AC fluctuations after rectification. With reduced leakage current, SP-TENG-B can minimize charge loss between cycles, which inherently smooths the DC output.

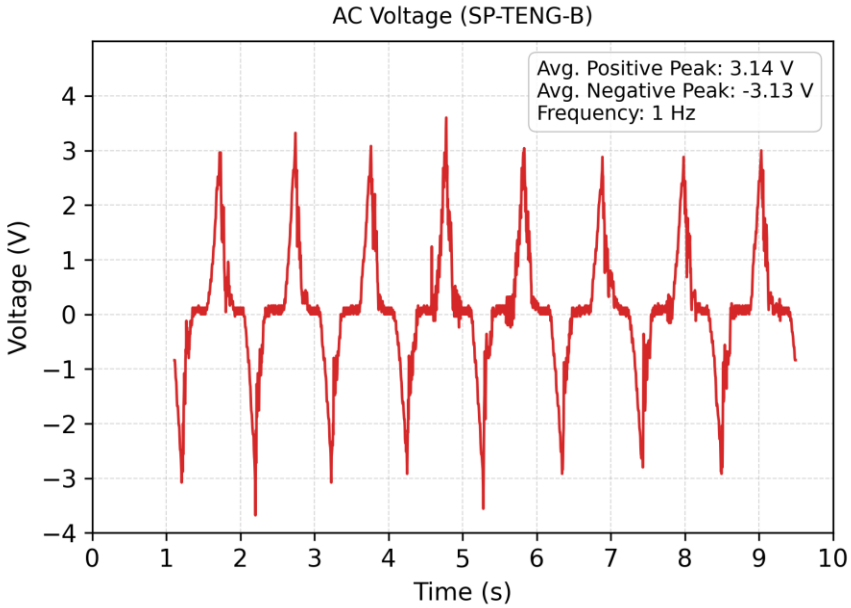

Figure 9.
AC Voltage of SP-TENG-B.

Edelweiss Applied Science and Technology
ISSN: 2576-8484
Vol. 9, No. 5: 2700-2716, 2025
DOI: 10.55214/25768484.v9i5.7585

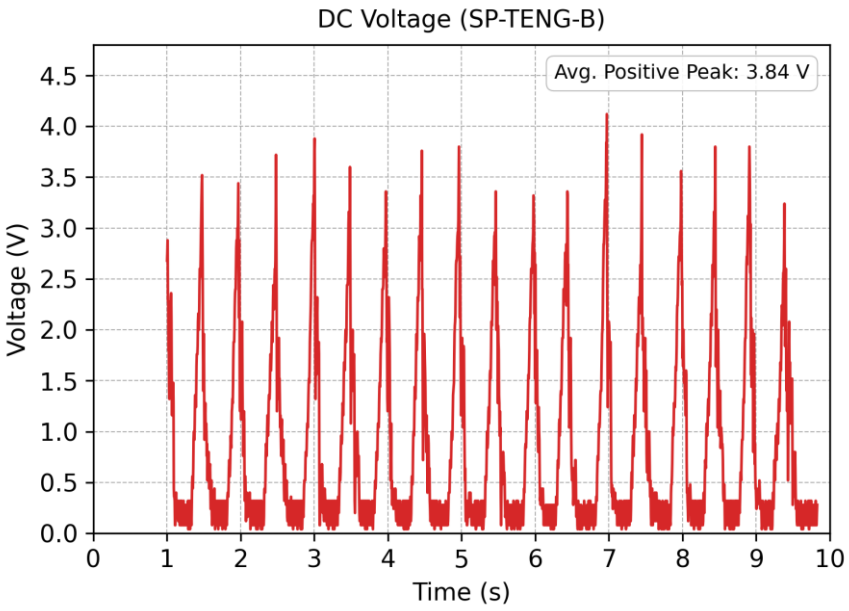

Figure 10.
DC Voltage of SP-TENG-B.

In addition, to evaluate the output performance of both SP-TENG devices, their ability to charge capacitors was tested. Capacitors with values of 10 µF, 22 µF, 47 µF, 100 µF, and 220 µF were used in the experiments. The voltage across each capacitor was recorded over time, with all charging curves monitored for at least 400 seconds. The charging performance of SP-TENG-A for different capacitors at 1 Hz sliding-–motion is shown in Figure 11. The charging voltage increases rapidly at the beginning, then gradually saturates over time. A 10 µF capacitors can be easily charged up to 1.2 V in 100 seconds. As the capacitor sizes and capacitance increases, the charging rates slow down. Capacitors with 22 µF, 47 µF and 100 µF reached their final voltages which is above 1.0 V but take longer to charge compared to the 10 µF. In contrast, 220 µF shows slowest charging rates and reaches only 0.78 V after 400 seconds due to its larger energy storage capacity.

On the other hand, Figure 12 demonstrated the charging performance of SP-TENG-B for different capacitors at 1 Hz sliding motion frequency. The capacitor charging curves for SP-TENG-B show improved output performance compared to SP-TENG-A. At a frequency of 1 Hz, the 10 µF and 22 µF capacitors reach higher voltages of around 1.9 V within 100 seconds. The 47 µF and 100 µF capacitors also show strong performance, both exceeding 1.7 V. With the largest capacitor, 220 µF can be charged steadily and reached about 1.45 V in 400 seconds which is almost double the performance of SP-TENG-A. Compared to SP-TENG-A, all capacitor sizes charge to higher final voltages in SP-TENG-B. However, the highest voltage of SP-TENG-B can reach is around 1.9 V, this happens because the charges on the PTFE plates have already been fully activated by the triboelectric effect and cannot generate more charge beyond that point.

Edelweiss Applied Science and Technology
ISSN: 2576-8484
Vol. 9, No. 5: 2700-2716, 2025
DOI: 10.55214/25768484.v9i5.7585

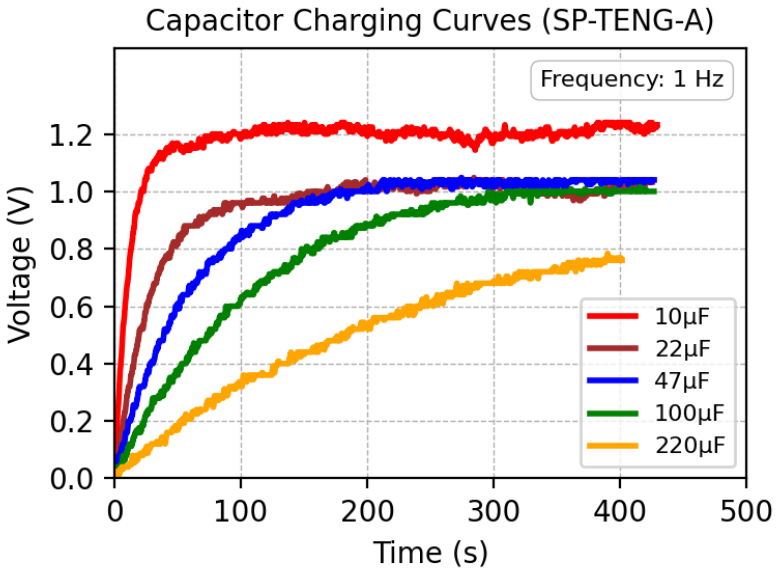

Figure 11.
Capacitor charging curves for SP-TENG-A over 400 s.

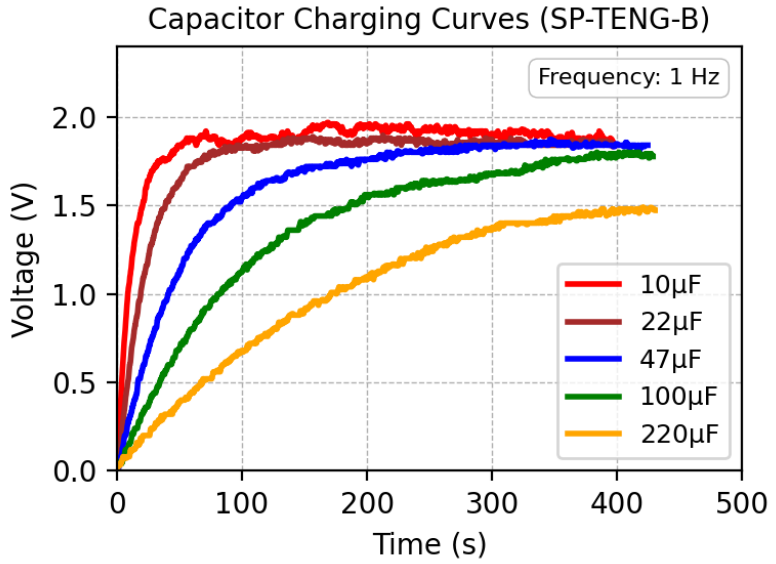

Figure 12.
Capacitor charging curves for SP-TENG-B over 400 s.

To better observe and compare the initial charging rates of both SP-TENG devices, the capacitor charging curves were re-plotted with a shorter time range of up to 60 seconds. Figure 13 shows the short-term capacitor charging behavior of the SP-TENG-A within the first 60 seconds at 1 Hz frequency sliding-motion. The 10 μF capacitor exhibits the fastest charging rate, it achieved over 1.1 V in 60 s. As the capacitance increases, the charging rate decreases. The 220 μF capacitor shows the slowest response, reaching only around 0.2 V at the end of 60 seconds. This behavior reflects the inverse relationship between capacitance and charging speed, where larger capacitors require more time and energy to accumulate voltage due to their higher storage capacity.

Edelweiss Applied Science and Technology
ISSN: 2576-8484
Vol. 9, No. 5: 2700-2716, 2025
DOI: 10.55214/25768484.v9i5.7585

On the other hand, Figure 14 demonstrates the capacitor charging curves for SP-TENG-B over 60 s under the same 1 Hz frequency sliding-motion. A 10 μF is charged up to 1.8 V in 60 s. While, the 220 μF capacitor is charged up to 0.4 V at the end of 60 seconds. As compared with SP-TENG-A, SP-TENG-B exhibits nearly double the charging rate for capacitors with 47 μF, 100 μF, and 220 μF. This indicates that SP-TENG-B has a higher charge transfer capability and energy harvesting performance. The improved performance may be due to stronger triboelectric interactions. Although SP-TENG-A incorporates an additional layer of PTFE coated on the fixed electrode, its output performance does not surpass that of SP-TENG-B, which uses solid PTFE plates. This is likely because the coated PTFE layer in SP-TENG-A may result in weaker contact electrification due to its reduced surface charge density and potential non-uniformities in coating thickness. In contrast, the solid PTFE plates in SP-TENG-B provide a more stable and consistent triboelectric interface, leading to enhanced charge transfer during contact-separation cycles. Consequently, SP-TENG-B achieves higher energy conversion efficiency, as reflected in its superior charging behavior across a range of capacitor values.

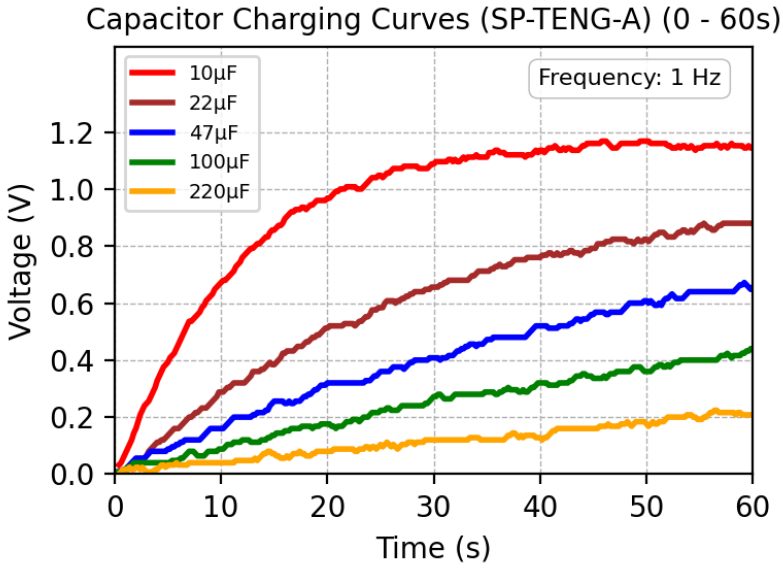

Figure 13.
Capacitor charging curves for SP-TENG-A over 60 s.

Edelweiss Applied Science and Technology
ISSN: 2576-8484
Vol. 9, No. 5: 2700-2716, 2025
DOI: 10.55214/25768484.v9i5.7585

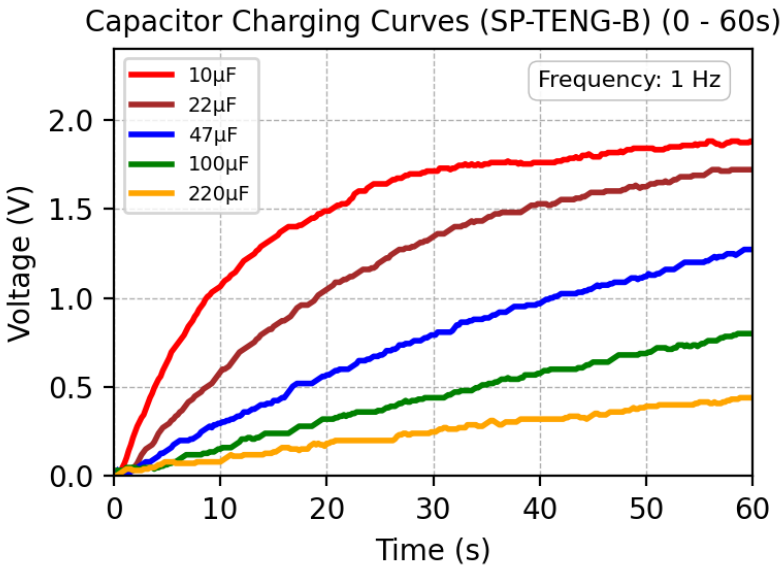

Figure 14.
Capacitor charging curves for SP-TENG-B over 60 s.

To demonstrate the practical application of the SP-TENG, SP-TENG-B was used to harvest low-frequency mechanical energy, then the generated energy is rectified and stored in a capacitor to power small electronic devices. This is because SP-TENG-B shows better output performance, allowing it to effectively harvest and deliver energy to devices such as LEDs and a digital timer. Figure 15 illustrates the number of LEDs illuminated by SP-TENG-B. The device is connected to a full-wave bridge rectifier, which converts the AC output into DC to power the LEDs connected in series. Under simulated wave excitation at a frequency of 1 Hz generated manually by sliding the PTFE plates, a total of 93 LEDs can be directly powered and illuminated. Each back-and-forth movement of the PTFE plates produces an electrical output sufficient to light up the LEDs momentarily. Figure 16 depicts the total number of LEDs illuminated by SP-TENG-B under night conditions.

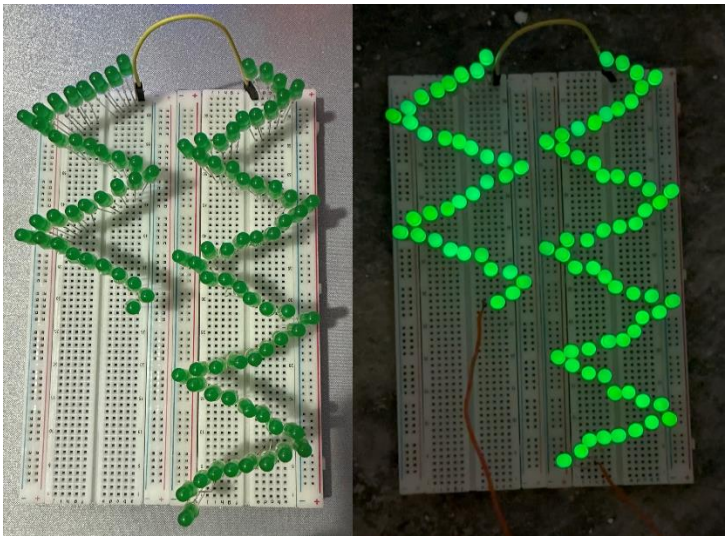

Figure 15.
Total number of LEDs illuminated by the SP-TENG-B.

Edelweiss Applied Science and Technology
ISSN: 2576-8484
Vol. 9, No. 5: 2700-2716, 2025
DOI: 10.55214/25768484.v9i5.7585

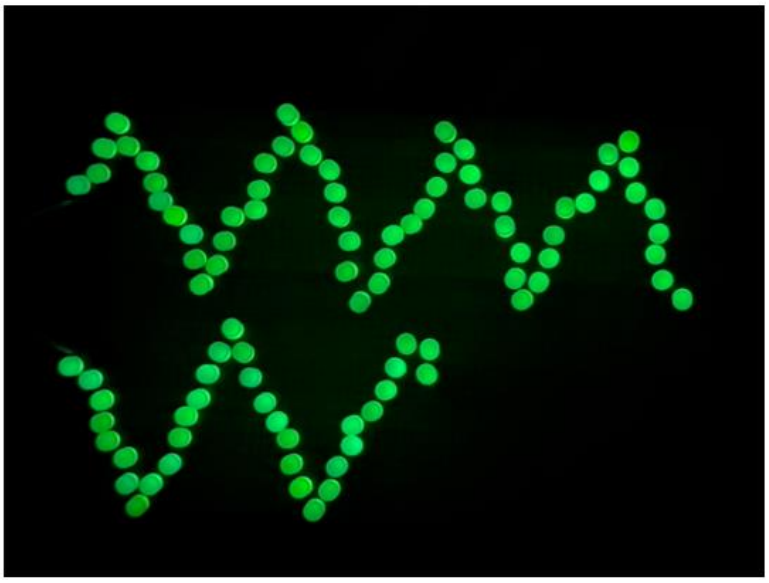

Figure 16.
Total number of LEDs illuminated by the SP-TENG-B under night conditions.

Additionally, a digital liquid crystal display (LCD) timer was successfully powered using the SP-TENG-B device. A 47 μF capacitor is connected through a full-wave bridge rectifier and then charged by SP-TENG-B. As shown in Figure 17, during the charging phase from 0 to 95 seconds, the SP-TENG-B gradually increases the capacitor voltage, reaching a peak of approximately 2.4 V. When the switch is turned on, the capacitor begins to discharge and the stored energy is used to power the LCD timer. Figure 18(a) shows the LCD screen illuminated during operation. However, as the capacitor discharged, the timer gradually faded and turned off. This indicates that while SP-TENG-A can power the device, its operating time is limited by the small capacitor size. The performance can be further improved by using a larger capacitor, allowing the LCD timer to function more continuously. Figure 18(b) shows the LCD timer gradually fading as the capacitor discharges.

Edelweiss Applied Science and Technology
ISSN: 2576-8484
Vol. 9, No. 5: 2700-2716, 2025
DOI: 10.55214/25768484.v9i5.7585

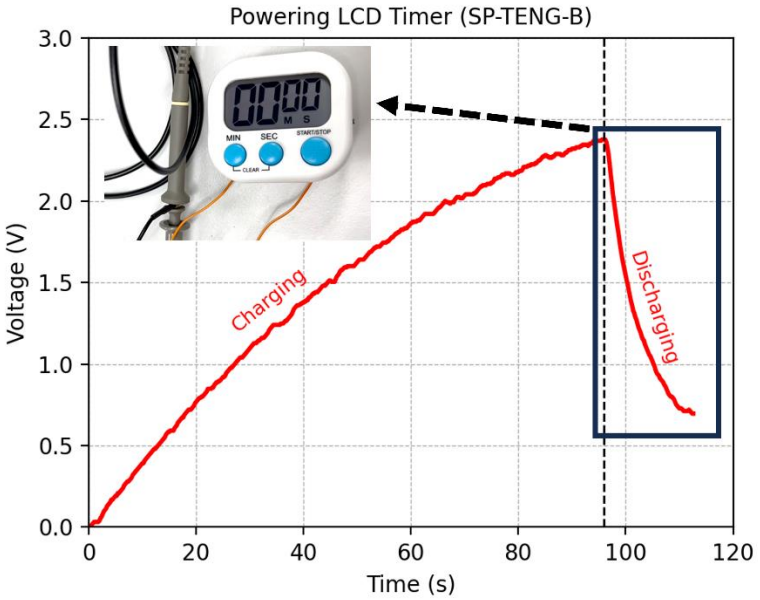

Figure 17.
Charging curves of LCD timer with SP-TENG-B.

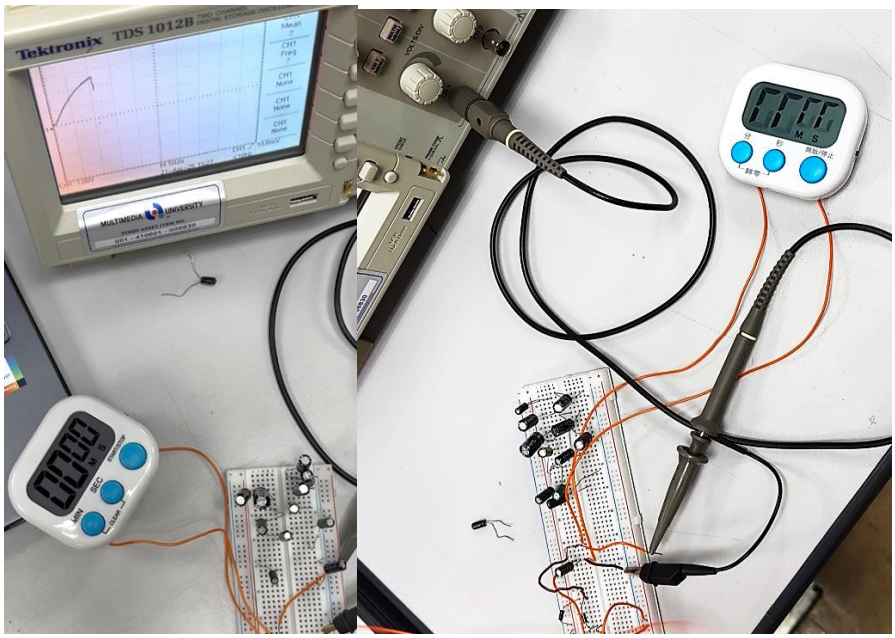

Figure 18.
(a) Powering LCD timer with SP-TENG-B.
(b) LCD timer gradually fading as the capacitor discharges.

4. Conclusion

In this work, a stackable pallet-shaped triboelectric nanogenerator is proposed as a water wave energy harvester. The stackable pallet TENG (SP-TENG) were fabricated into two different configurations. SP-TENG-A consists of two fixed aluminum electrodes coated with PTFE layers and

Edelweiss Applied Science and Technology
ISSN: 2576-8484
Vol. 9, No. 5: 2700-2716, 2025
DOI: 10.55214/25768484.v9i5.7585

aluminum-coated sliding plates as moving electrodes. On the other hand, SP-TENG-B consists with two fixed aluminum electrodes and solid PTFE sliding plates. Through the manual-sliding motion, both SP-TENG device effectively harvest mechanical energy at low-frequency, mimicking the water wave motion. The output performance of both designs, each with 11 layers has been studied. After optimizing the design parameters, SP-TENG-B demonstrated not only a simpler fabrication process but also superior electrical output compared to SP-TENG-A. The solid PTFE plates in SP-TENG-B played a key role in enhancing performance by generating higher charge density and improving contact area during sliding. Additionally, the parallel connection of each layer was found to be the optimal configuration for maximizing both voltage and current output from the stacked structure. Under the excitation of the sliding motion as in actual wave condition, SP-TENG-B achieved a maximum output of 4 V. In application testing, SP-TENG-B successfully powered 93 LEDs and a digital timer. The result proved its ability to charge energy storage units and drive low-power electronic devices. In summary, SP-TENG exhibits multiple advantages such as modular structure, space efficiency, and simple fabrication. It shows great potential for future applications in harvesting low-frequency wave energy in marine or coastal environments.

Transparency:

The authors confirm that the manuscript is an honest, accurate, and transparent account of the study; that no vital features of the study have been omitted; and that any discrepancies from the study as planned have been explained. This study followed all ethical practices during writing.

Copyright:

References

[1] E. Callaway, "Energy: To catch a wave," *Nature*, vol. 450, no. 7167, pp. 156–159, 2007. https://doi.org/10.1038/450156a

[2] T. Jiang and Z. L. Wang, "High Efficient and High Durability Triboelectric Nanogenerators for Blue Energy," *Handbook of Triboelectric Nanogenerators*, pp. 1-34, 2023. https://doi.org/10.1007/978-3-031-05722-9_39-1

[3] B. Drew, A. R. Plummer, and M. N. Sahinkaya, *A review of wave energy converter technology*. London, England: Sage Publications Sage UK, 2009.

[4] A. F. d. O. Falcão, "Wave energy utilization: A review of the technologies," *Renewable and Sustainable Energy Reviews*, vol. 14, no. 3, pp. 899-918, 2010. https://doi.org/https://doi.org/10.1016/j.rser.2009.11.003

[5] Z. Lin, W. Long, L. J. Chen, S. Niu, and Y. Zi, *Triboelectric nanogenerators*. Springer. https://doi.org/10.1007/978-3-319-40039-6, 2016.

[6] S. Li *et al.*, "Manipulating the triboelectric surface charge density of polymers by low-energy helium ion irradiation/implantation," *Energy & Environmental Science*, vol. 13, no. 3, pp. 896-907, 2020. https://doi.org/10.1039/C9EE03307F

[7] A. Haroun, M. Tarek, M. Mosleh, and F. Ismail, "Recent progress on triboelectric nanogenerators for vibration energy harvesting and vibration Sensing," *Nanomaterials*, vol. 12, no. 17, p. 2960, 2022.

[8] B. Shi *et al.*, "Progress in recent research on the design and use of triboelectric nanogenerators for harvesting wind energy," *Nano Energy*, vol. 116, p. 108789, 2023. https://doi.org/https://doi.org/10.1016/j.nanoen.2023.108789

[9] N. Satpute *et al.*, "Triboelectric nanogenerator-based vibration energy harvester using bio-inspired microparticles and mechanical motion amplification," *Energies*, vol. 16, no. 3, p. 1315, 2023. https://doi.org/10.3390/en16031315

[10] J. Wang *et al.*, "Rational structure optimized hybrid nanogenerator for highly efficient water wave energy harvesting," *Advanced Energy Materials*, vol. 9, no. 8, p. 1802892, 2019. https://doi.org/https://doi.org/10.1002/aenm.201802892

[11] Y. Dong *et al.*, "Gas-liquid two-phase flow-based triboelectric nanogenerator with ultrahigh output power," *Science Advances*, vol. 8, no. 48, p. eadd0464, 2022. https://doi.org/10.1126/sciadv.add0464

[12] J. Liu, S. Ciampi, and A. Antony, *The origins of solid-solid contact electrification. In Z. L. Wang, Y. Yang, J. Zhai, & J. Wang (Eds.), Handbook of Triboelectric Nanogenerators*. Springer International Publishing. https://doi.org/10.1007/978-3-031-28111-2_2, 2023.

[13] Y. Lu *et al.*, "Liquid-liquid triboelectric nanogenerator based on the immiscible interface of an aqueous two-phase system," *Nature Communications*, vol. 13, no. 1, p. 5316, 2022. https://doi.org/10.1038/s41467-022-33086-2

[14] D. Choi, D. Yoo, K. J. Cha, M. La, and D. S. Kim, "Spontaneous occurrence of liquid-solid contact electrification in nature: Toward a robust triboelectric nanogenerator inspired by the natural lotus leaf," *Nano Energy*, vol. 36, pp. 250-259, 2017. https://doi.org/https://doi.org/10.1016/j.nanoen.2017.04.026

[15] S. Xu *et al.*, "Gas-solid two-phase flow-driven triboelectric nanogenerator for wind-sand energy harvesting and self-powered monitoring sensor," *Nano Energy*, vol. 85, p. 106023, 2021. https://doi.org/https://doi.org/10.1016/j.nanoen.2021.106023

[16] Z. L. Wang and A. C. Wang, "On the origin of contact-electrification," *Materials Today*, vol. 30, pp. 34-51, 2019. https://doi.org/https://doi.org/10.1016/j.mattod.2019.05.016

[17] H. Zhai, S. Ding, X. Chen, Y. Wu, and Z. L. Wang, "Advances in solid–solid contacting triboelectric nanogenerator for ocean energy harvesting," *Materials Today*, vol. 65, pp. 166-188, 2023. https://doi.org/https://doi.org/10.1016/j.mattod.2023.02.030

[18] J. Shao, M. Willatzen, Y. Shi, and Z. L. Wang, "3D mathematical model of contact-separation and single-electrode mode triboelectric nanogenerators," *Nano Energy*, vol. 60, pp. 630-640, 2019. https://doi.org/https://doi.org/10.1016/j.nanoen.2019.03.072

[19] S. Amini, R. F. Sagade Muktar Ahmed, S. Madanahalli Ankanathappa, and K. Sannathammegowda, "Polyaniline-doped textile-based triboelectric nanogenerator: Self-powered device for wearable electronics," *Applied Research*, vol. 4, no. 1, p. e202400124, 2025. https://doi.org/https://doi.org/10.1002/appl.202400124

[20] S. Wang, L. Lin, Y. Xie, Q. Jing, S. Niu, and Z. L. Wang, "Sliding-triboelectric nanogenerators based on in-plane charge-separation mechanism," *Nano Letters*, vol. 13, no. 5, pp. 2226-2233, 2013. https://doi.org/10.1021/nl400738p

[21] W.-Z. Song *et al.*, "Sliding mode direct current triboelectric nanogenerators," *Nano Energy*, vol. 90, p. 106531, 2021. https://doi.org/https://doi.org/10.1016/j.nanoen.2021.106531

[22] G. M. Rani, S. M. Ghoreishian, R. Umapathi, V. Vivekananthan, and Y. S. Huh, "A biocompatible triboelectric nanogenerator-based edible electronic skin for morse code transmitters and smart healthcare applications," *Nano Energy*, vol. 128, p. 109899, 2024. https://doi.org/https://doi.org/10.1016/j.nanoen.2024.109899

[23] S. Nuthalapati *et al.*, "Wearable High-Performance MWCNTs/PDMS Nanocomposite based Triboelectric Nanogenerators for Haptic Applications," *IEEE Journal on Flexible Electronics*, vol. 9, no. 3, pp. 393–400, 2024. https://doi.org/10.1109/JFLEX.2024.3446756

[24] S. Wang, Y. Xie, S. Niu, L. Lin, and Z. L. Wang, "Freestanding triboelectric-layer-based nanogenerators for harvesting energy from a moving object or human motion in contact and non-contact modes," *Advanced Materials*, vol. 26, no. 18, pp. 2818-2824, 2014. https://doi.org/10.1002/adma.201305303

[25] K. J. M. A. Alnabi and L. Lee, "Freestanding triboelectric-layer mode triboelectric nanogenerator (TENG) via rotating circle," *International Journal of Integrated Engineering*, vol. 16, no. 3, pp. 133–144, 2024. https://doi.org/10.30880/ijie.2024.16.03.013

[26] H. Wang *et al.*, "Sandwich-like triboelectric nanogenerators integrated self-powered buoy for navigation safety," *Nano Energy*, vol. 84, p. 105920, 2021. https://doi.org/https://doi.org/10.1016/j.nanoen.2021.105920

[27] H. Wang *et al.*, "A stackable triboelectric nanogenerator for wave-driven marine buoys," *Nanomaterials*, vol. 12, no. 4, p. 594, 2022. https://doi.org/10.3390/nano12040594

[28] Z. Zhang *et al.*, "Multi-tunnel triboelectric nanogenerator for scavenging mechanical energy in marine floating bodies," *Journal of Marine Science and Engineering*, vol. 10, no. 4, p. 455, 2022. https://doi.org/10.3390/jmse10040455

[29] Y. Duan *et al.*, "Scalable rolling-structured triboelectric nanogenerator with high power density for water wave energy harvesting toward marine environmental monitoring," *Nano Research*, vol. 16, no. 9, pp. 11646-11652, 2023. https://doi.org/10.1007/s12274-023-6035-x

[30] S. Pan and Z. Zhang, "Fundamental theories and basic principles of triboelectric effect: A review," *Friction*, vol. 7, pp. 2-17, 2019.